

Room-temperature magnetic higher-order topological states in two-dimensional transition metal dichalcogenides and dihalogenides

Chenqiang Hua,^{1,2,*} Dexi Shao,³ Weikang Wu,⁴ Wenjin Gao^{①,1,5} Meimei Wu,¹ Guoxiang Zhi,² Tianchao Niu,¹ Shengyuan A. Yang,⁶ and Miao Zhou^{①,2,5,†}

¹Hangzhou International Innovation Institute, *Beihang University*, Hangzhou 311115, China

²Tianmushan Laboratory, Hangzhou 311115, China

³School of Physics, *Hangzhou Normal University*, Hangzhou 311115, China

⁴Key Laboratory for Liquid-Solid Structural Evolution and Processing of Materials, Ministry of Education, *Shandong University*, Jinan 250061, China

⁵School of Physics, *Beihang University*, Beijing 100191, China

⁶Research Laboratory for Quantum Materials, IAPME, *University of Macau*, Macau 999078, China



(Received 9 May 2024; revised 6 July 2024; accepted 22 July 2024; published 7 August 2024)

Higher-order topological insulators (HOTIs) have attracted significant interest in recent years due to their unique properties, but the material realization is mainly limited to nonmagnetic systems. In this work, through tight-binding modeling and first-principles calculations, we reveal the experimentally synthesized two-dimensional (2D) VSe_2 as an example of a room-temperature magnetic HOTI. The nontrivial nature is characterized by an inverted band feature with a large gap and spin-polarized corner states with quantized fractional charge. We demonstrate that the topological corner states are robust against magnetization canting, defects, and strain, suggesting the great potential for experimental detection. Remarkably, the magnetic HOTI phase can be extended to other 2D dichalcogenides and dihalogenides, including VX_2 , ScX'_2 , YX'_2 , RuX'_2 ($X = S, Se, Te$; $X' = Cl, Br, I$) as well as their Janus structures. Our work not only provides a series of promising candidates for room-temperature magnetic HOTIs, but also sheds light on future design and regulation of novel quantum states for real applications.

DOI: [10.1103/PhysRevB.110.085413](https://doi.org/10.1103/PhysRevB.110.085413)

I. INTRODUCTION

The discovery of topological insulators has opened up one of the most active fields in physics and materials science over the past two decades [1–5]. In recent years, a focus of this field is on higher-order topological insulators (HOTIs). For a two-dimensional (2D) HOTI, both its bulk and one-dimensional (1D) edges are gapped, whereas protected gapless modes appear at its zero-dimensional corners [6]. This is different from conventional topological insulators in two dimensions, which feature topological gapless modes at 1D edges [1,6]. 2D HOTIs were discovered first in nonmagnetic 2D materials with preserved time-reversal symmetry, such as graphdiyne and graphynes [7–9], the MoS_2 family [10], and many others [11–14]. Recently, with the experimental realization of 2D magnetic materials, there is an increasing interest to extend the exploration of 2D HOTIs to magnetic systems. So far, a few candidates have been theoretically predicted, including bismuthene on $EuO(111)$ [15], $FeSe$ [16], $Co_3(HITP)_2$ [17], $RuCl_2$ [18], $CrOCl$ [19,20], $CrSiTe_3$ [20], $CrSBr$ [21], and VS_2 [22]. However, so far experimental characterizations of magnetic HOTI states are rare. For most predicted systems, they have a quite low magnetic transition temperature that is

disadvantageous for experimental detection and future applications.

Transition metal dichalcogenides and dihalogenides represent a large family of solid-state materials [23–26]. They often have stable or metastable structures with a layered geometry, and many of them exhibit magnetic ordering due to the partially filled d shells [27–40]. Notably, some members of this family can maintain a high magnetic transition temperature in 2D form [27,28,40]. VSe_2 is a typical example that has been experimentally synthesized [40]. It adopts 2H structure with a ferromagnetic (FM) order, and the Curie temperature (T_c) is above room temperature (~ 420 K) even down to the monolayer limit [40]. Plenty of intriguing properties have been revealed in the VSe_2 family, such as structural phase transition, quantum size effect, large anomalous Hall effect, and intrinsic valley polarization [31–39].

In this work, we demonstrate 2D 2H- VSe_2 as the first example of a room-temperature magnetic HOTI, which has sizable gaps for both bulk and edges. Through first-principles calculations, we reveal that the nontrivial band topology originates from band inversion in one of the two spin channels. According to a C_3 -symmetry-enabled invariant, the topology is characterized, and the quantized corner charge is identified to be $\frac{e}{3}$. For an open nanodisk, gapless corner modes are explicitly demonstrated, which are strongly spin polarized. We construct a tight-binding (TB) model to capture the key features of the magnetic HOTI state in this system, and

*Contact author: huachenqiang@buaa.edu.cn

†Contact author: mzhou@buaa.edu.cn

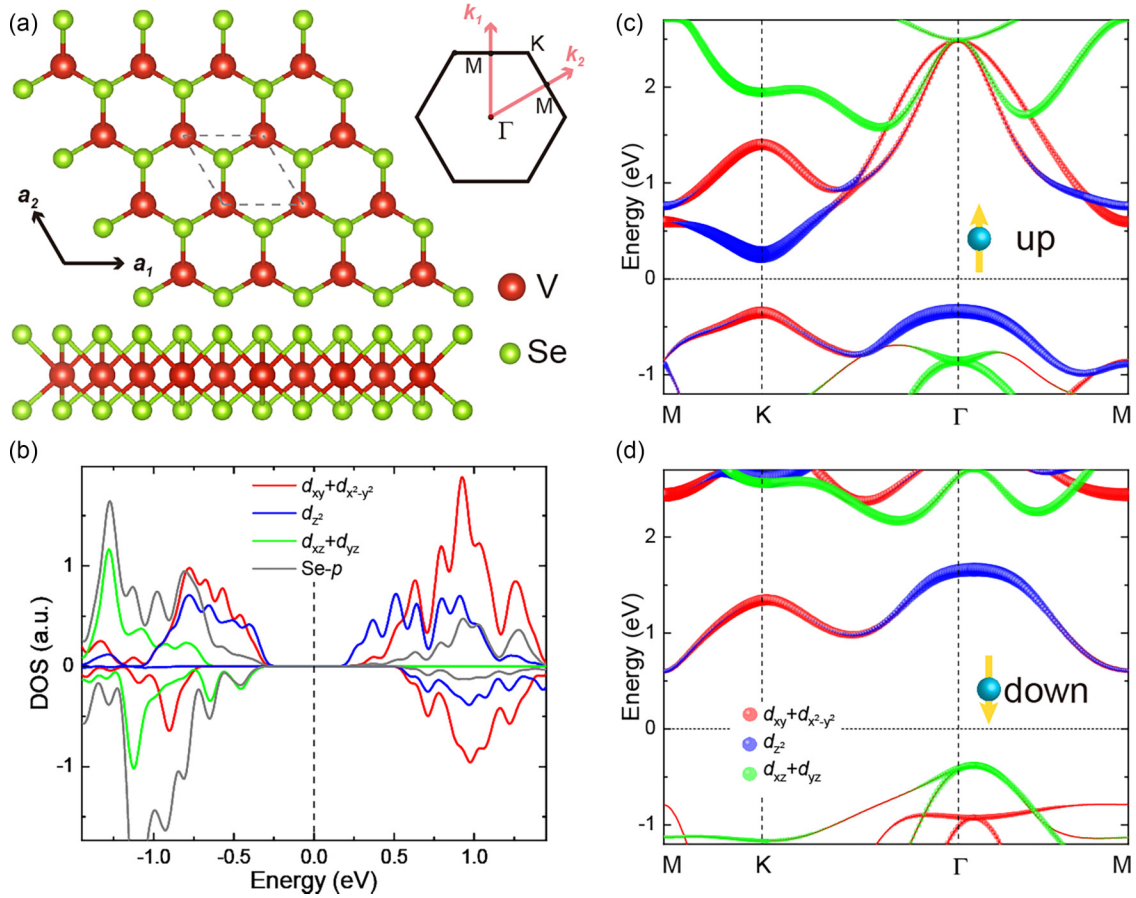


FIG. 1. Atomic structure and electronic properties of 2H-VSe₂. (a) Atomic structure of 2D VSe₂. The Brillouin zone with high-symmetry points is indicated in the inset. (b) Partial DOS projected onto the $d_{xy} + d_{x^2-y^2}$, d_{z^2} , and $d_{xz} + d_{yz}$ orbitals of V and p orbitals of Se. [(c), (d)] Projected band structures for spin-up and down channels, respectively. Fermi level is set to zero.

effects of spin-orbit coupling (SOC), magnetization direction, defects, and strain are also discussed. Furthermore, we find that the HOTI phase is shared by a series of sister compounds of VSe₂, including VX₂, ScX'₂, YX'₂ and RuX'₂ ($X = S, Se, Te$; $X' = Cl, Br, I$), as well as their related Janus structures.

II. METHODS

Our first-principles calculations were based on density functional theory (DFT) by using the Vienna Ab Initio Simulation Package [41]. The projector augmented wave method was used to capture the ion-electron interactions [42]. The exchange-correlation functional was modeled by the generalized gradient approximation (GGA) in Perdew-Burke-Ernzerhof (PBE) format [43]. A vacuum region of 20 Å was used to eliminate artificial interactions between periodic images. The energy cutoff was taken to be 500 eV. The k meshes for structural optimization and electronic structure calculations were set to $13 \times 13 \times 1$ and $17 \times 17 \times 1$, respectively. The convergence criteria for energy and force were set to 1×10^{-6} eV and 0.01 eV/Å, respectively. The rotationally invariant DFT+ U method was used to capture the correlation effects of d orbitals [44] and the values are listed in Table S1 in the Supplemental Material [45]. For VSe₂, we took the effective U parameter to be 2.41 eV, which was obtained from previous calculations using constrained random-phase

approximation [46]. For other systems, the effective U values were estimated within the linear response method [47]. Using VSe₂ as a benchmark, the adopted U values are quite close to those used in previous studies [18,48–51]. To calculate the topological invariant, we extracted the irreducible representations of occupied states by using the topological quantum chemistry method [52], as implemented in irvsp [53]. To compute the edge and corner modes, Wannier TB models were constructed based on the DFT band structures [54,55].

III. RESULTS AND DISCUSSION

A. Crystal structure and band properties

Like most transition metal dichalcogenides, VSe₂ has a layered crystal structure. Previous experiments [33] have shown that in the bulk form, VSe₂ adopts the 1T structure, whereas when its thickness is decreased to a few layers or a monolayer, the 2H structure is more favored. The atomic structure of 2D VSe₂ is shown in Fig. 1(a), which has a space group of $P\bar{6}m2$ (point group D_{3h}). The optimized lattice constant is $a = 3.374$ Å, agreeing well with the previous results [32,35,39]. Due to the presence of the 3d element V with partially filled d shells, it exhibits strong ferromagnetism. Interestingly, experiments have shown that 2D VSe₂ has a high T_c of 420 K [40], while the T_c predicted by *ab initio* calculations can reach 590 K [39].

We then focus on the electronic structures of monolayer VSe₂. The calculated density of states (DOS) and electronic band structures are shown in Figs. 1(b)–1(d). One can see that the system is a spin-polarized semiconductor. The band gap in the spin-up (spin-down) channel is about 0.60 eV (0.98 eV), in accordance with previous reports [32,35,39]. We project DOS onto the 3*d* orbitals of V and *p* orbitals of Se, and find that both conduction- and valence-band edges are dominated by V *d* orbitals. In the 2H structure, each V ion is surrounded by six Se anions with a trigonal prismatic coordination. By symmetry, it splits the *d* orbitals of V into three groups, *A*₁ (*d*_{z²}) singlet, and *E* (*d*_{xy}, *d*_{x²-y²}) and *E'* (*d*_{xz}, *d*_{yz}) doublets. In the spin-polarized band structures as shown in Figs. 1(c) and 1(d), the weights of the three groups for each Bloch state are plotted. Near Fermi level, one can see that for the spin-up channel, a single *d* band with characteristics of *d*_{xy}, *d*_{x²-y²}, and *d*_{z²} orbitals is fully occupied, while this band is empty in the spin-down channel. This is consistent with the nominal valence of the V ion being +4, and agrees with the calculated magnetic moment of 1μ_B on V with *d*¹ configuration.

One notes that, in the spin-up channel [Fig. 1(c)], the conduction and valence bands near the band gap show a mixture of *A*₁(*d*_{z²}) and *E*(*d*_{xy}, *d*_{x²-y²}) characteristics. This mixing is allowed by the horizontal mirror symmetry *M*_z of the structure. Interestingly, careful examination of the distribution of *A*₁ and *E* components in Fig. 1(c) reveals a band inversion at the *K* (*K'*) point. The occupied *d* bands are mainly composed of *A*₁(*d*_{z²}), but around *K* (*K'*) the orbital overlaps with the conduction band and the main contribution changes to *E*(*d*_{xy}, *d*_{x²-y²}). This band inversion hints at nontrivial topology.

B. Edge and corner modes

To directly characterize the topological properties of 2D VSe₂, we calculate the topological invariant, edge, and corner states. For each spin channel, the material can be regarded as a spinless system with an effective time-reversal symmetry. For a *C*₃-symmetric system, the topological invariant is defined in terms of eigenvalues. With each spin channel *s* = ↑, ↓, we can calculate its invariant by [56]

$$Q_s^{(3)} = \frac{e}{3} [K_2^{(3)}] \text{ mod } e, \quad (1)$$

where *e* is the electron charge, and $[K_p^{(3)}]$ is the number difference of occupied states with *C*₃ eigenvalue $\exp[\frac{2\pi(p-1)i}{3}]$ between *C*₃-invariant points *K* and Γ . By extracting the eigenvalues from DFT band structures (see Table S2 [45]), we find that $Q_{\uparrow}^{(3)} = \frac{e}{3}$ and $Q_{\downarrow}^{(3)} = 0$ for the spin-up and spin-down channels, respectively, as listed in Table I. This indicates that in terms of $Q_s^{(3)}$ invariant, the spin-up channel is topologically nontrivial, whereas the spin-down channel is trivial. This is consistent with the band-structure calculations with band inversion occurring only in the spin-up channel, whereas the spin-down channel shows no band inversion.

Previously, it was shown that a nonzero $Q^{(3)}$ invariant must lead to a filling anomaly with corner charge for a *C*₃-symmetric system without gapless edge modes [56–58]. We confirm this by calculating the edge spectrum of a semifinite ribbon by using Wannier functions (see the Wannier fitted

TABLE I. Calculated secondary topological index $[K_2^{(3)}]$ and topological invariant $Q^{(3)}$. *n* denotes the number of occupied bands.

System	Spin	<i>n</i>	$[K_2^{(3)}]$	$Q^{(3)}$	System	Spin	<i>n</i>	$[K_2^{(3)}]$	$Q^{(3)}$
VSe ₂	up	13	1	$\frac{e}{3}$	VSSe	up	13	1	$\frac{e}{3}$
	down	12	0	0		down	12	0	0
RuBr ₂	up	16	0	0	RuClBr	up	16	0	0
	down	12	1	$\frac{e}{3}$		down	12	1	$\frac{e}{3}$

band structure in Fig. S1 [45]). The calculated results are plotted in Fig. 2(a). One observes that the edge states are fully gapped. The calculated gap size is 0.13 eV, much larger than the thermal fluctuation at room temperature.

The fractional corner charge described by $Q^{(3)}$ corresponds to the existence of topological corner modes. To verify this, we construct a triangular nanodisk that respects *C*₃ symmetry and the side length is ~5 nm. Figure 2(b) shows the calculated eigenvalues for this disk. Clearly, inside the bulk gap one can see two pairs of isolated modes. By checking their wavefunction distributions, we find that these states are strongly localized at the corners [see Figs. 2(c) and 2(d)], which are topological corner modes. Furthermore, these modes are spin-up polarized, consistent with our analysis above that the spin-up channel is nontrivial while the spin-down channel is trivial. The filling anomaly requires that if the whole system maintains charge neutrality, the corner modes must be fractionally occupied. Indeed, the calculated charge at each corner is $\frac{e}{3}$. These results confirm that 2D VSe₂ is a room-temperature magnetic HOTI.

C. Effective TB model

The key ingredient to achieve nontrivial topology in 2D VSe₂ lies in the band inversion between the *A*₁ (*d*_{z²}) singlet and *E*(*d*_{xy}, *d*_{x²-y²}) doublet in the spin-up channel. To understand the underlying physics, we construct a low-energy spinless Hamiltonian describing *d*_{z²}, *d*_{xy}, and *d*_{x²-y²} orbitals of V. The hoppings between neighboring sites are described in terms of the Slater-Koster parameters [59]. The Fourier-transformed model in momentum space takes the form

$$\mathcal{H} = \begin{bmatrix} H_E & T \\ T^\dagger & H_{A_1} \end{bmatrix}, \quad (2)$$

where *H*_{*E*} and *H*_{*A*₁} are 2×2 and 1×1 blocks describing the hopping processes among *E* doublet and *A*₁ singlet, respectively. *T* is the 2×1 block describing the hopping between *E* and *A*₁. The detailed expressions of these blocks are presented in the Supplemental Material [45].

In 2D VSe₂, the *E* doublet has an energy higher than *A*₁, which can be seen from the energy ordering at Γ in Fig. 1. In Eq. (2), this is captured by assigning a higher on-site energy for *E* than that of *A*₁. In Fig. 3(a), we put *T* = 0, so the one *A*₁ band and two *E* bands are decoupled. In this case, the *A*₁ band crosses the lower *E* band without hybridization, resulting in a nodal line in the Brillouin zone. Now, if we include the hopping *T*, the crossing point will be gapped, and we can obtain an insulator state when the filling number is 1 [see Fig. 3(b)]. Interestingly, the calculated lowest *C*₃

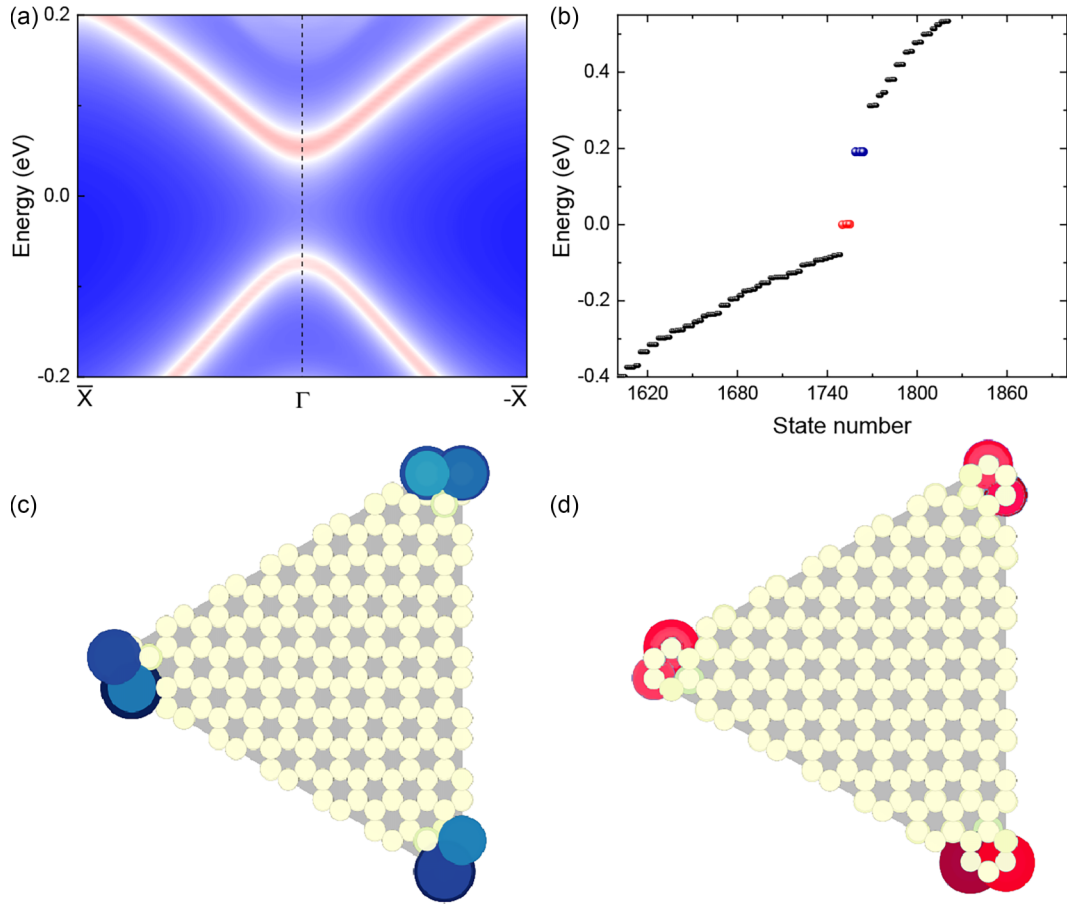


FIG. 2. Spin-polarized edge and corner states of 2D VSe_2 . (a) Spectrum of the edge states. The edge modes near the Fermi level are spin-up polarized. (b) Eigenvalue of a triangular nanodisk, where only the spin-up channel can be seen. The blue and red dots denote the corner states. [(c), (d)] Spatial distribution of the corner states.

eigenvalue is $\exp[\frac{2\pi i}{3}]$ at the K point, while the eigenvalue is 1 at Γ , reflecting a band inversion feature. For the band structure shown in Fig. 3(b), we can also compute $Q^{(3)}$ and find that $Q^{(3)} = \frac{\epsilon}{3}$. We have further calculated the topological corner modes and the distributions in real space [Fig. 3(c)], reproducing the DFT results for the spin-up channel in 2D VSe_2 . These results suggest that the simple TB model captures well the essential features of the magnetic HOTI state in VSe_2 .

D. Robustness of corner states

Next, we explore the robustness of corner states. As the low-energy bands in 2D VSe_2 are mainly derived from the $3d$ orbitals of V, which typically have weak SOC strength, one may expect that SOC should not have a strong influence on the electronic properties. Indeed, we have calculated the band structures with SOC and find that the system is still a semiconductor, with a band gap of ~ 0.52 eV [see Fig. 4(a)]. The low-energy bands have dispersions similar to those obtained

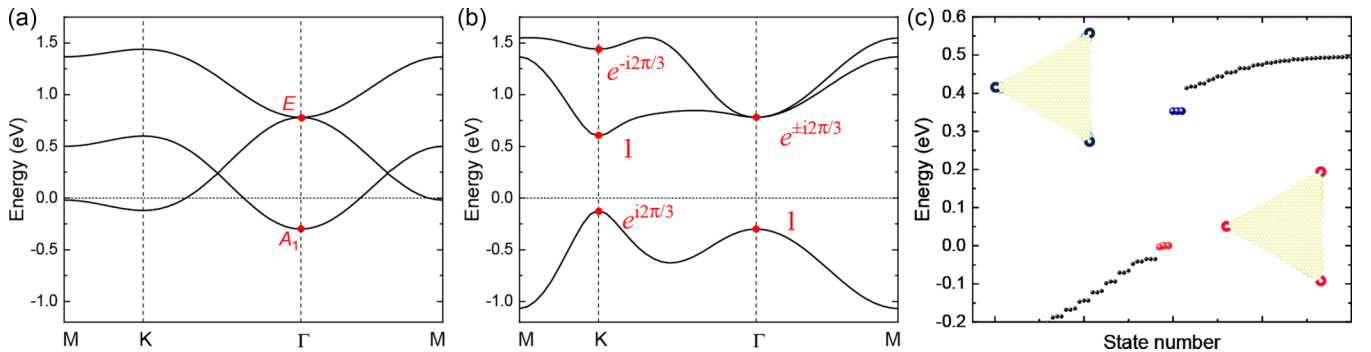


FIG. 3. Effective TB model. (a) TB band structure without the off-diagonal T block. (b) TB band structure with the off-diagonal T block. (c) Eigenvalue of a triangular nanodisk. The blue and red dots denote the corner states. Insets: Spatial distribution of the corner states. $V_{dd\sigma} = -0.19$, $V_{dd\pi} = 0.187$, $V_{dd\delta} = -0.07$, $E_a = -0.30$, $E_b = -0.70$, $t_2 = 0.30$; (a) $t_4 = 0$ and (b) $t_4 = -0.37$.

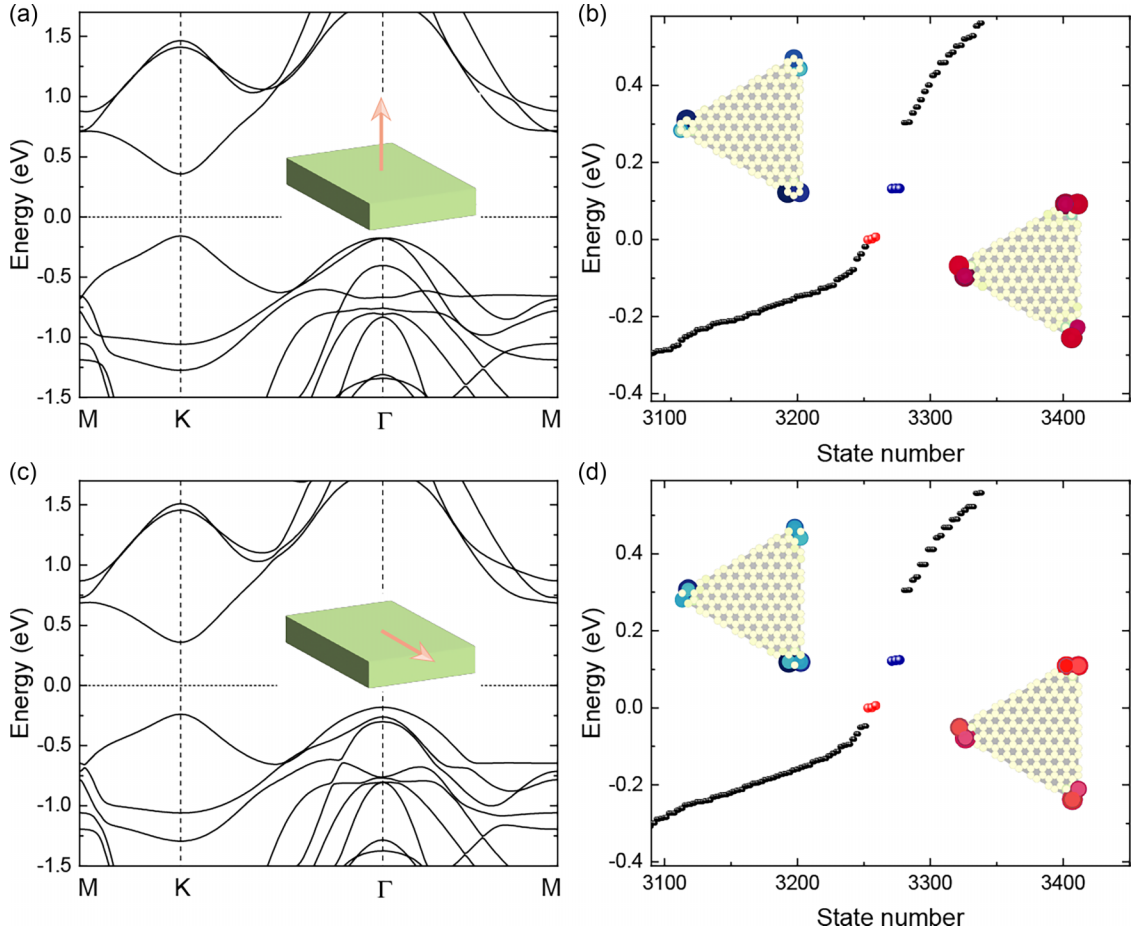


FIG. 4. Band structures and topological corner properties of VSe₂ with the inclusion of SOC. (a) Band structure when magnetization direction is out of plane. (b) Eigenvalue of a triangular nanodisk with out-of-plane magnetization. (c) Band structure when magnetization direction is in plane. (d) Eigenvalue of a triangular nanodisk with in-plane magnetization. Fermi level is set to zero. The blue and red dots denote the corner states. Insets: Schematic of the magnetization direction and spatial distribution of the corner states.

without SOC (Fig. 1). In Fig. 4(a), we take the magnetization to be out of plane (along the z direction). This configuration preserves the C_3 symmetry, so we can still use the C_3 eigenvalues to characterize the band inversion. With SOC, the two spin channels are coupled and need to be considered simultaneously. Now the $Q^{(3)}$ invariant can be evaluated by the formula [57]

$$Q^{(3)} = -\frac{e}{3}([K_1^{(3)}] + [K_2^{(3)}]) \bmod e. \quad (3)$$

Here, for a spinful system, $[X_p^{(3)}]$ ($X = K/K'$) is the number difference of occupied states with C_3 eigenvalue $\exp[\frac{\pi(2p-1)i}{3}] \exp(\frac{\pi i}{3})$ between C_3 -invariant points K and Γ . The calculated C_3 eigenvalues are listed in Table S2 [45], where $[K_1^{(3)}]$ and $[K_2^{(3)}]$ are determined to be -1 and 3 , respectively. As a result, we can obtain $Q^{(3)} = \frac{e}{3}$, the same as the total $Q^{(3)}$ (i.e., the sum of the two spin channels) of 2D VSe₂ in the absence of SOC (Table I). This confirms that the weak SOC in VSe₂ does not change the band inversion feature. In Fig. 4(b), we plot the spectrum of eigenvalues for the same triangle-shaped sample as presented in Fig. 2(b). One can see that the in-gap corner modes persist with SOC, and these modes are strongly spin polarized.

Energetically, it was shown that monolayer VSe₂ favors an in-plane magnetization [36]. For such a configuration, $Q^{(3)}$ is not well defined since the C_3 symmetry is broken. Nevertheless, as the SOC effect is weak, the corner modes should still exist and evolve continuously from those in Fig. 4(b). We have calculated the band structure with in-plane magnetization. As shown in Fig. 4(c), the band gap remains almost intact compared to that with out-of-plane magnetization. One can still observe the spin-polarized in-gap corner modes [see Fig. 4(d)]. Therefore, we can safely conclude that the weak SOC does not affect the existence of topological corner modes.

In practice, material samples normally have defects and impurities. Previous reports have explored the effects of defects on the corner modes, revealing that the topological states are not sensitive to defects that are not too close to the corners [12]. Here, to demonstrate the robustness of corner states in 2D VSe₂, we introduce a hole at the central, side, or edge region of the triangular nanodisk (see Fig. S2 [45]). It should be noted that, when the hole is located at the side or edge region of the disk, the global C_3 symmetry will be broken. Nevertheless, it is found that although electronic defect states emerge in the spectrum of eigenvalues due to the presence of a hole, the topological corner states could still be identified,

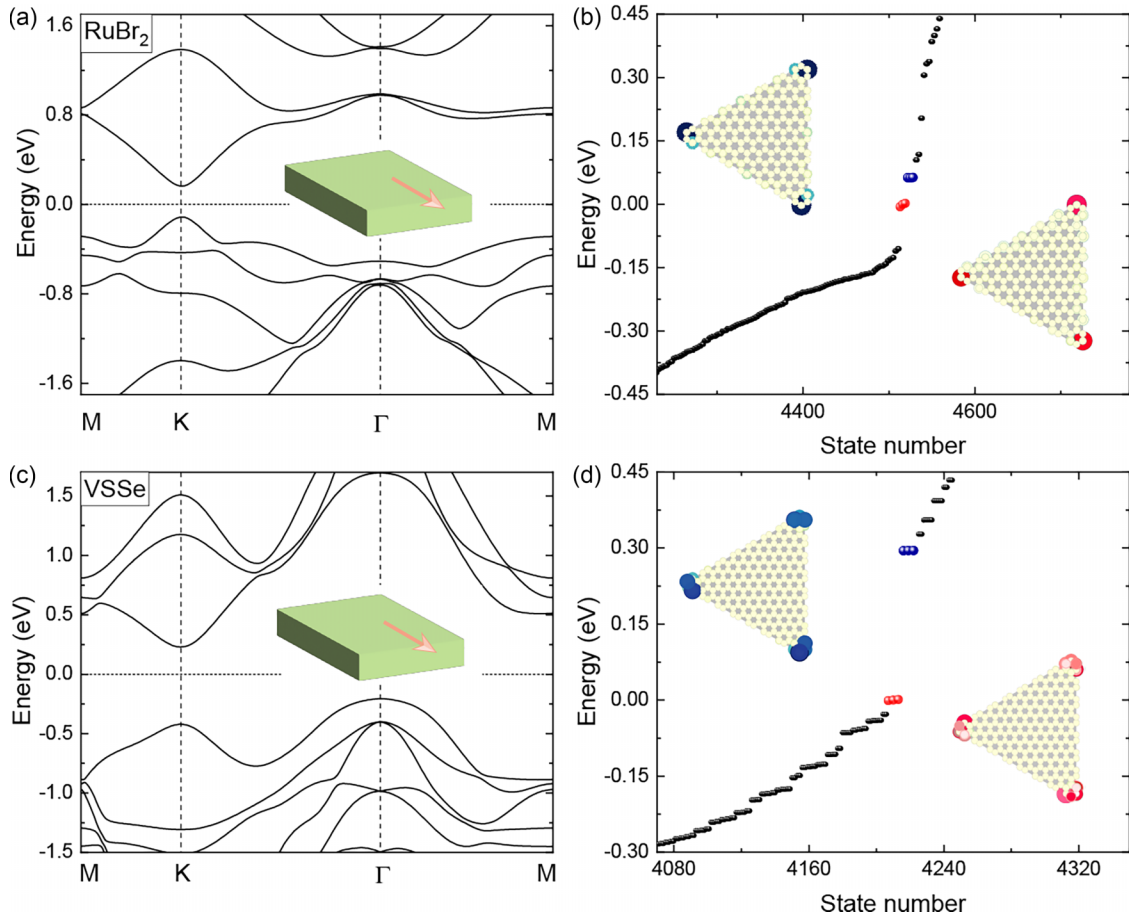


FIG. 5. Band structures and corner states of 2D RuBr_2 and VSSe . (a) Band structure of RuBr_2 with SOC. The magnetization direction is in plane. (b) Eigenvalue of a triangular nanodisk. (c) Band structure of VSSe . (d) Eigenvalue. Fermi level is set to zero. The blue and red dots denote the corner states. Insets: Schematic of the magnetization direction and spatial distribution of the corner states.

no matter whether the system has in-plane or out-of-plane magnetization (Fig. S2 [45]). Furthermore, we have considered the effect of disk size on the corner states (see Fig. S3 [45]), and the stability of corner states against strain is also explored (Fig. S4 [45]). The results clearly suggest that the topological corner states in VSe_2 are robust against magnetization canting, defects, disk size, and strain.

E. Discussion

We have demonstrated that 2D VSe_2 is a room-temperature magnetic HOTI. Its high Curie temperature and sizable band gap are beneficial for experimental detection. In experiment, one may probe the topological corner states using scanning tunneling spectroscopy (STS) [12,13]. By comparing the results measured at the corners and in the bulk, it is able to distinguish the corner states that appear as sharp peaks in the spectrum. In addition, the spin-polarized characteristics of the corner modes can be detected by using a magnetic tip as implemented in spin-polarized STS.

Finally, we demonstrate that the magnetic HOTI phase is in fact shared by other 2D transition metal dichalcogenides and dihalogenides, including VX_2 , ScX'_2 , YX'_2 ($X = \text{S, Se, Te}$; $X' = \text{Cl, Br, I}$) as well as their Janus structures (see Fig. S5

and Table S3 [45]). It is also plausible to achieve a HOTI phase by preparing compounds with metal ions having d^6 configuration, such as RuX'_2 , in which five d electrons occupy the spin-up bands, while the remaining d electron fills one of the spin-down bands. The calculated band structure of RuBr_2 is presented in Fig. 5(a), and the spectrum of eigenvalues for a triangular nanodisk exhibits two pairs of corner modes as shown in Fig. 5(b), distinctly revealing a HOTI phase. For a Janus structure of transition metal dichalcogenide or dihalogenide, the space group symmetry is reduced to $P3m1$ but the C_3 symmetry is preserved. Therefore, the topological behaviors should be similar to their parent counterparts. Taking VSSe as an example, we have computed the band structure and corner states [Figs. 5(c) and 5(d)], which are very similar to those of VSe_2 . For the corner charge, we verify the fractional quantization for RuBr_2 , VSSe , and RuClBr (see Table I). We have also shown that the topological invariant $Q^{(3)}$ equals $\frac{e}{3}$ for other systems, including VS_2 , VTe_2 , RuCl_2 , RuI_2 , ScCl_2 , ScBr_2 , ScI_2 , YCl_2 , YBr_2 , YI_2 , VSeTe , and RuBrI (see details in Table S3 [45]). The findings could not only broaden the candidates for magnetic HOTI phase, but also provide an exciting playground to regulate the exotic quantum states for multifunctionalities.

IV. CONCLUSIONS

In conclusion, we have established an example of room-temperature 2D magnetic HOTI. We uncover that 2D VSe_2 , which has been synthesized in experiments with a high T_c of ~ 420 K, exhibits a nontrivial higher-order band topology. The physical origin is traced back to the singly occupied d bands in the spin majority channel, where band inversion occurs, while the spin minority channel is trivial. The key features of band structure are captured by a simplified three-band model that describes well the electronic properties and may serve as a general picture for other structures. The associated topological corner states are explicitly demonstrated, which are robust against magnetization canting, defects, and strain. Importantly, the proposed magnetic HOTIs can be extended

to other members of 2D transition metal dichalcogenides and dihalogenides, greatly facilitating the experimental detection and future applications of novel quantum states in experimentally available materials.

ACKNOWLEDGMENTS

This work is supported by the Natural Science Foundation of Zhejiang Province (Grants No. LQ23A040013 and No. LZ22A040004), the National Natural Science Foundation of China (Grants No. 11674042 and No. 12204029), and the Fundamental Research Funds for the Central Universities. We also acknowledge the support from the High-performance Computing Centre in Hangzhou International Innovation Institute of Beihang University.

-
- [1] P. Liu, J. R. Williams, and J. J. Cha, Topological nanomaterials, *Nat. Rev. Mater.* **4**, 479 (2019).
- [2] M. Z. Hasan and C. L. Kane, *Colloquium: Topological insulators*, *Rev. Mod. Phys.* **82**, 3045 (2010).
- [3] B. A. Bernevig, C. Felser, and H. Beidenkopf, Progress and prospects in magnetic topological materials, *Nature (London)* **603**, 41 (2022).
- [4] Y. Tokura, K. Yasuda, and A. Tsukazaki, Magnetic topological insulators, *Nat. Rev. Phys.* **1**, 126 (2019).
- [5] X.-L. Qi and S.-C. Zhang, Topological insulators and superconductors, *Rev. Mod. Phys.* **83**, 1057 (2011).
- [6] B. Xie, H.-X. Wang, X. Zhang, P. Zhan, J.-H. Jiang, M. Lu, and Y. Chen, Higher-order band topology, *Nat. Rev. Phys.* **3**, 520 (2021).
- [7] B. Liu, G. Zhao, Z. Liu, and Z. F. Wang, Two-dimensional quadrupole topological insulator in γ -graphyne, *Nano Lett.* **19**, 6492 (2019).
- [8] E. Lee, R. Kim, J. Ahn, and B.-J. Yang, Two-dimensional higher-order topology in monolayer graphdiyne, *npj Quantum Mater.* **5**, 1 (2020).
- [9] X.-L. Sheng, C. Chen, H. Liu, Z. Chen, Z.-M. Yu, Y. X. Zhao, and S. A. Yang, Two-dimensional second-order topological insulator in graphdiyne, *Phys. Rev. Lett.* **123**, 256402 (2019).
- [10] J. Jung and Y. H. Kim, Hidden breathing kagome topology in hexagonal transition metal dichalcogenides, *Phys. Rev. B* **105**, 085138 (2022).
- [11] Z. Guo, J. Deng, Y. Xie, and Z. Wang, Quadrupole topological insulators in $Ta_2M_3Te_5$ ($M = Ni, Pd$) monolayers, *npj Quantum Mater.* **7**, 87 (2022).
- [12] S. N. Kempkes, M. R. Slot, J. J. van den Broeke, P. Capiod, W. A. Benalcazar, D. Vanmaekelbergh, D. Bercioux, I. Swart, and C. Morais Smith, Robust zero-energy modes in an electronic higher-order topological insulator, *Nat. Mater.* **18**, 1292 (2019).
- [13] T. Hu, W. Zhong, T. Zhang, W. Wang, and Z. F. Wang, Identifying topological corner states in two-dimensional metal-organic frameworks, *Nat. Commun.* **14**, 7092 (2023).
- [14] X. Ni, H. Huang, and J. L. Brédas, Organic higher-order topological insulators: Heterotriangulene-based covalent organic frameworks, *J. Am. Chem. Soc.* **144**, 22778 (2022).
- [15] C. Chen, Z. Song, J.-Z. Zhao, Z. Chen, Z.-M. Yu, X.-L. Sheng, and S. A. Yang, Universal approach to magnetic second-order topological insulator, *Phys. Rev. Lett.* **125**, 056402 (2020).
- [16] A. Luo, Z. Song, and G. Xu, Fragile topological band in the checkerboard antiferromagnetic monolayer FeSe, *npj Comput. Mater.* **8**, 26 (2022).
- [17] X. Zhang, T. He, Y. Liu, X. Dai, G. Liu, C. Chen, W. Wu, J. Zhu, and S. A. Yang, Magnetic real Chern insulator in 2D metal-organic frameworks, *Nano Lett.* **23**, 7358 (2023).
- [18] R. Li, N. Mao, X. Wu, B. Huang, Y. Dai, and C. Niu, Robust second-order topological insulators with giant valley polarization in two-dimensional honeycomb ferromagnets, *Nano Lett.* **23**, 91 (2023).
- [19] Z. Guo, Y. Liu, H. Jiang, X. Zhang, L. Jin, C. Liu, and G. Liu, Magnetic high-order topological insulator in 2D layered $CrOCl$, *Mater. Today Phys.* **36**, 101153 (2023).
- [20] X. Wang, X. Li, J. Li, C. Xie, J. Wang, H. Yuan, W. Wang, Z. Cheng, Z. Yu, and G. Zhang, Magnetic second-order topological insulator: An experimentally feasible 2D $CrSiTe_3$, *Adv. Funct. Mater.* **33**, 2304499 (2023).
- [21] Z. Guo, H. Jiang, L. Jin, X. Zhang, G. Liu, Y. Liu, and X. Wang, Second-order topological insulator in ferromagnetic monolayer and antiferromagnetic bilayer $CrSBr$, *Small Sci.* **4**, 2300356 (2024).
- [22] G. Liu, H. Jiang, Z. Guo, X. Zhang, L. Jin, C. Liu, and Y. Liu, Magnetic second-order topological insulators in 2H-transition metal dichalcogenides, *Adv. Sci.* **10**, 2301952 (2023).
- [23] S. Manzeli, D. Ovchinnikov, D. Pasquier, O. V. Yazyev, and A. Kis, 2D transition metal dichalcogenides, *Nat. Rev. Mater.* **2**, 17033 (2017).
- [24] V. Ortiz Jimenez, Y. T. H. Pham, D. Zhou, M. Liu, F. A. Nugera, V. Kalappattil, T. Eggers, K. Hoang, D. L. Duong, M. Terrones, H. Rodriguez Gutiérrez, and M. H. Phan, Transition metal dichalcogenides: Making atomic-level magnetism tunable with light at room temperature, *Adv. Sci.* **11**, 2304792 (2024).
- [25] W. Choi, N. Choudhary, G. H. Han, J. Park, D. Akinwande, and Y. H. Lee, Recent development of two-dimensional transition metal dichalcogenides and their applications, *Mater. Today* **20**, 116 (2017).
- [26] M. Xu, T. Liang, M. Shi, and H. Chen, Graphene-like two-dimensional materials, *Chem. Rev.* **113**, 3766 (2013).
- [27] M. Bonilla, S. Kolekar, Y. Ma, H. C. Diaz, V. Kalappattil, R. Das, T. Eggers, H. R. Gutierrez, M.-H. Phan, and M. Batzill, Strong room-temperature ferromagnetism in VSe_2 monolayers on van der Waals substrates, *Nat. Nanotechnol.* **13**, 289 (2018).

- [28] X. Zhang, Q. Lu, W. Liu, W. Niu, J. Sun, J. Cook, M. Vaninger, P. F. Miceli, D. J. Singh, S. W. Lian, T. R. Chang, X. He, J. Du, L. He, R. Zhang, G. Bian, and Y. Xu, Room-temperature intrinsic ferromagnetism in epitaxial CrTe₂ ultrathin films, *Nat. Commun.* **12**, 2492 (2021).
- [29] H. Y. Lv, W. J. Lu, D. F. Shao, Y. Liu, and Y. P. Sun, Strain-controlled switch between ferromagnetism and antiferromagnetism in $1T - CrX_2$ ($X = Se, Te$) monolayers, *Phys. Rev. B* **92**, 214419 (2015).
- [30] M. Ashton, D. Gluhovic, S. B. Sinnott, J. Guo, D. A. Stewart, and R. G. Hennig, Two-dimensional intrinsic half-metals with large spin gaps, *Nano Lett.* **17**, 5251 (2017).
- [31] A. H. M. A. Wasey, S. Chakrabarty, and G. P. Das, Quantum size effects in layered VX₂ ($X = S, Se$) materials: Manifestation of metal to semimetal or semiconductor transition, *J. Appl. Phys.* **117**, 064313 (2015).
- [32] H. Zhang, L. M. Liu, and W. M. Lau, Dimension-dependent phase transition and magnetic properties of VS₂, *J. Mater. Chem. A* **1**, 10821 (2013).
- [33] D. Li, X. Wang, C. Kan, D. He, Z. Li, Q. Hao, H. Zhao, C. Wu, C. Jin, and X. Cui, Structural phase transition of multilayer VSe₂, *ACS Appl. Mater. Interfaces* **12**, 25143 (2020).
- [34] M. Esters, R. G. Hennig, and D. C. Johnson, Dynamic instabilities in strongly correlated VSe₂ monolayers and bilayers, *Phys. Rev. B* **96**, 235147 (2017).
- [35] H.-R. Fuh, B. Yan, S.-C. Wu, C. Felser, and C.-R. Chang, Metal-insulator transition and the anomalous Hall effect in the layered magnetic materials VS₂ and VSe₂, *New J. Phys.* **18**, 113038 (2016).
- [36] J. Liu, W.-J. Hou, C. Cheng, H.-X. Fu, J.-T. Sun, and S. Meng, Intrinsic valley polarization of magnetic VSe₂ monolayers, *J. Phys.: Condens. Matter* **29**, 255501 (2017).
- [37] F. Li, K. Tu, and Z. Chen, Versatile electronic properties of VSe₂ bulk, few-layers, monolayer, nanoribbons, and nanotubes: A computational exploration, *J. Phys. Chem. C* **118**, 21264 (2014).
- [38] M. Hossain, H. Zhang, Y. Huangfu, M. Z. Saeed, B. Qin, D. Bloos, and X. Duan, 2D metallic vanadium dichalcogenides and related heterostructures, *Mater. Today Adv.* **21**, 100451 (2024).
- [39] H. Pan, Electronic and magnetic properties of vanadium dichalcogenides monolayers tuned by hydrogenation, *J. Phys. Chem. C* **118**, 13248 (2014).
- [40] X. Wang, D. Li, Z. Li, C. Wu, C. M. Che, G. Chen, and X. Cui, Ferromagnetism in 2D vanadium diselenide, *ACS Nano* **15**, 16236 (2021).
- [41] G. Kresse and J. Furthmüller, Efficient iterative schemes for *ab initio* total-energy calculations using a plane-wave basis set, *Phys. Rev. B* **54**, 11169 (1996).
- [42] P. E. Blöchl, Projector augmented-wave method, *Phys. Rev. B* **50**, 17953 (1994).
- [43] J. P. Perdew, K. Burke, and M. Ernzerhof, Generalized gradient approximation made simple, *Phys. Rev. Lett.* **77**, 3865 (1996).
- [44] A. I. Liechtenstein, V. I. Anisimov, and J. Zaanen, Density-functional theory and strong interactions: Orbital ordering in Mott-Hubbard insulators, *Phys. Rev. B* **52**, R5467 (1995).
- [45] See Supplemental Material at <http://link.aps.org/supplemental/10.1103/PhysRevB.110.085413> for details about additional information on TB modeling; Wannier fitted bands of VSe₂; robustness of corner states against defects, disk size, and strain; and spin-polarized band structures for other systems.
- [46] A. Karbalaei Aghaee, S. Belbasi, and H. Hadipour, *Ab initio* calculation of the effective Coulomb interactions in MX₂ ($M = Ti, V, Cr, Mn, Fe, Co, Ni; X = S, Se, Te$): Intrinsic magnetic ordering and Mott phase, *Phys. Rev. B* **105**, 115115 (2022).
- [47] M. Cococcioni and S. de Gironcoli, Linear response approach to the calculation of the effective interaction parameters in the LDA+*U* method, *Phys. Rev. B* **71**, 035105 (2005).
- [48] H. Sun, S.-S. Li, W.-X. Ji, and C.-W. Zhang, Valley-dependent topological phase transition and quantum anomalous valley Hall effect in single-layer RuClBr, *Phys. Rev. B* **105**, 195112 (2022).
- [49] D. Dey and A. S. Botana, Structural, electronic, and magnetic properties of vanadium-based Janus dichalcogenide monolayers: A first-principles study, *Phys. Rev. Mater.* **4**, 074002 (2020).
- [50] H. L. Zhuang and R. G. Hennig, Stability and magnetism of strongly correlated single-layer VS₂, *Phys. Rev. B* **93**, 054429 (2016).
- [51] Z. Guan and S. Ni, Predicted 2D ferromagnetic Janus VSeTe monolayer with high Curie temperature, large valley polarization and magnetic crystal anisotropy, *Nanoscale* **12**, 22735 (2020).
- [52] M. G. Vergniory, B. J. Wieder, L. Elcoro, S. S. P. Parkin, C. Felser, B. A. Bernevig, and N. Regnault, All topological bands of all nonmagnetic stoichiometric materials, *Science* **376**, 816 (2022).
- [53] J. Gao, Q. Wu, C. Persson, and Z. Wang, Irvsp: To obtain irreducible representations of electronic states in the VASP, *Comput. Phys. Commun.* **261**, 107760 (2021).
- [54] Q. Wu, S. Zhang, H.-F. Song, M. Troyer, and A. A. Soluyanov, WannierTools: An open-source software package for novel topological materials, *Comput. Phys. Commun.* **224**, 405 (2018).
- [55] A. A. Mostofi, J. R. Yates, G. Pizzi, Y.-S. Lee, I. Souza, D. Vanderbilt, and N. Marzari, An updated version of wannier90: A tool for obtaining maximally-localised Wannier functions, *Comput. Phys. Commun.* **185**, 2309 (2014).
- [56] W. A. Benalcazar, T. Li, and T. L. Hughes, Quantization of fractional corner charge in C_n -symmetric higher-order topological crystalline insulators, *Phys. Rev. B* **99**, 245151 (2019).
- [57] R. Takahashi, T. Zhang, and S. Murakami, General corner charge formula in two-dimensional C_n -symmetric higher-order topological insulators, *Phys. Rev. B* **103**, 205123 (2021).
- [58] F. Schindler, M. Brzezińska, W. A. Benalcazar, M. Iraola, A. Bouhon, S. S. Tsirkin, M. G. Vergniory, and T. Neupert, Fractional corner charges in spin-orbit coupled crystals, *Phys. Rev. Res.* **1**, 033074 (2019).
- [59] J. C. Slater and G. F. Koster, Simplified LCAO method for the periodic potential problem, *Phys. Rev.* **94**, 1498 (1954).